Parametric control of thermal self-pulsation in micro-cavities

Article (Accepted Version)

Parametric Control of Thermal Self-Pulsation in Micro-Cavities

LUIGI DI LAURO,[1] JIN LI,[2] DAVID J. MOSS,[3] ROBERTO MORANDOTTI,[4,5,6] SAI T. CHU,[2] MARCO PECCIANTI,[1] ALESSIA PASQUAZI[1,*]

[1] *Emergent Photonics Lab (EPic), Department of Physics and Astronomy, University of Sussex, Falmer, Brighton, BN1 9QH, United Kingdom.*
[2] *City University of Hong Kong, Kowloon Tong, Hong Kong.*
[3] *Centre for Microphotonics, Swinburne University of Technology, Hawthorn, VIC 3122, Australia.*
[4] *INRS-EMT, 1650 Boulevard Lionel-Boulet, Varennes, Québec, Canada J3X 1S2.*
[5] *Institute of Fundamental and Frontier Sciences, University of Electronic Science and Technology of China, Chengdu 610054, China.*
[6] *National Research University of Information Technologies, Mechanics and Optics, St Petersburg, Russia.*
**Corresponding author: a.pasquazi@sussex.ac.uk*

Received XX Month XXXX; revised XX Month, XXXX; accepted XX Month XXXX; posted XX Month XXXX (Doc. ID XXXXX); published XX Month XXXX

We propose a scheme for bifurcation control in micro-cavities based on the interplay between the ultrafast Kerr effect and a slow nonlinearity, such as thermo-optical, free-carriers or opto-mechanical nonlinearity. We demonstrate that Hopf bifurcations can be efficiently controlled with a low energy signal via four-wave mixing. Our results show that new strategies are possible for designing efficient micro-cavity based oscillators and sensors. Moreover, they provide new understanding on the effect of coherent wave mixing in the thermal stability regions of optical micro-cavities, fundamental for micro-cavity based applications in communications, sensing and metrology, including optical micro-combs.

OCIS codes: *(140.3945) Microcavities; (190.4380) Nonlinear optics, four-wave mixing; (190.3100) Instabilities and chaos; (190.4870) Photothermal effects; (190.1450) Bistability.*

http://dx.doi.org/10.1364/OL.99.099999

The interplay between slow and fast nonlinearities in optical micro-cavities [1-2] has attracted considerable attention in the last two decades [1-6]. Thanks to the micro-cavities' ability of strongly enhancing the optical field, bi-stable, self-pulsing (SP) and chaotic regimes can be observed at low powers [3,4]. Starting from the pioneering works in whispering-gallery mode resonators by Il' Chencko and co-workers [3], thermal oscillators have been studied in micro-cavities having different geometries. They are usually modelled with one or two temporal relaxation constants [3,4,7-9]. Amongst other effects, regenerative self-pulsing [10] and giant self-pulsation [11] have been reported, with applications, for example, to sensing [12]. In the generation of micro-combs [13] the control of the thermo-optical nonlinearity is fundamental for reaching coherent regimes, such as temporal cavity solitons. [14-16].

In semiconductor cavities, the free-carrier nonlinearity has a typical time response in the microsecond regime [6,17,18] and its contribution to self-pulsing regimes has been studied under different conditions [19], including with pulsed excitation [20].

Finally, opto-mechanical nonlinearities have also been efficiently employed for designing oscillators in the microwave regime [21]. Recently, Monifi et al. [5] have experimentally demonstrated control and transfer of nonlinear dynamics and chaos between two cavity modes via mechanical oscillation.

In this framework, the control of multi-stable or self-pulsing regions, usually arising at a bifurcation in the parameter space, is critical for achieving the desired performance. Specifically, relocating a bifurcation at a desired parameter value is a general problem in applied nonlinear science that has been approached with different methods [22].

In this letter, we study the effect of a parametric interaction, specifically four-wave mixing (FWM), on the nonlinear dynamics of a micro-cavity based oscillator exhibiting both Kerr nonlinearity and an intensity-dependent nonlinearity with a first order time-response, such as a thermal nonlinearity. We propose a configuration where a weak signal controls the self-oscillatory behavior of a strong pump. The stability regions of the system are dramatically modified even at very low signal powers, allowing such oscillations to be turned off and on, as well as controlled in amplitude and shape. Our results provide a new understanding of the thermal stability regions of a micro-cavity device that is particularly important for micro-comb generation [14-16, 23-24], especially in a bi-chromatic pumped configuration [23]. Moreover, they provide new degrees of freedom for designing efficient self-pulsing devices for sensing and microwave photonics applications.

For modelling our system, we use coupled mode theory [25]: a pump (0) and a signal (1), with amplitudes $s_{(0,1)}(t)$ and frequencies $\omega_{(0,1)}$ respectively, are injected into two resonances $\omega^R_{(0,1)}$ of an optical cavity, exciting the intra-cavity fields $a_{(0,1)}(t)$. They generate an idler $a_{-1}(t)$ and frequency $\omega_{-1} = 2\omega_0 - \omega_1$ via degenerate FWM. We use a dimensionless normalization of the temporal variable t against the photon life time τ_{ph}, so that $t\ \tau_{ph}$ provides the physical time in seconds. The optical amplitudes are normalized against a Kerr constant $\Gamma_K = \omega_0 c\ n_2/(V_{eff} n_{eff}^2)$, where c is the speed of light, V_{eff} the effective mode volume and n_2 and n_{eff} the Kerr and effective refractive indices, respectively. Here $|s_{(0,1)}\ /\sqrt{2\Gamma_{\mathrm{K}}}|^2$ represents the coupled power in [W] for the pump and signal respectively, while $s_{-1} = 0$. The equations are:

$$\frac{d\boldsymbol{a}_i}{dt} = -\boldsymbol{a}_i - i[\,\boldsymbol{\delta}_i + \boldsymbol{\Delta} - (2\boldsymbol{I}_T - |\boldsymbol{a}_i|^2)]\boldsymbol{a}_i + i\boldsymbol{F}_i - i\,\boldsymbol{s}_i, \quad (1)$$

where the FMW terms are $F_0 = 2\ a_0^* a_1 a_{-1}$ and $F_{\pm1} = a_0^2 a_{\mp1}^*$. The total energy in the cavity is $I_T = \Sigma_{k=0,\pm1} I_k$, with $I_i = |a_i|^2$, while $P_i = |s_i|^2$ and $\delta_i = (\omega_i^R - \omega_i)\tau_{ph}$ are the normalized intra-cavity energies, coupled powers and frequency detunings respectively. The detuning Δ due to the slow nonlinearity, is governed by:

$$\boldsymbol{\sigma}\frac{d\boldsymbol{\Delta}}{dt} = -\boldsymbol{\Delta} - \boldsymbol{\rho}\ \boldsymbol{I}_T, \quad (2)$$

with σ being the normalized relaxation time and ρ the effective nonlinear coefficient normalized against Γ_K. Such a model is a prototypical example for time-dependent nonlinearities and provides a general understanding for a large class of devices. Moreover, it reproduces accurately the thermal relaxation in micro-cavities [3,16], with a time response τ_T and a nonlinear thermo-optical index n_2^T resulting in $\sigma = \tau_T/\tau_{ph}$ and $\rho = n_2^T/n_2$. The parameter σ depends on the quality factor and can be engineered. Crystalline high Q resonators can easily have σ of the order of few tens, while integrated resonators with a lower Q-factor and a higher relaxation constant can have σ up to several orders of magnitude. The values for ρ are usually in the range of one to three orders of magnitude and can exhibit both signs [1-3].

We start by analyzing the stability of the steady state solution that can be obtained via standard linear perturbation analysis [26] calculating the eigenvalues of the perturbed stationary state. In the following examples, we choose $\sigma = 50$ and $\rho = -10$.

Fig. 1 (a,c) shows, as an example, the numerically evaluated regions for positive eigenvalues (unstable, US), eigenvalues with negative real part (stable, S) and with a positive real part and non-null imaginary part (self-pulsing, SP), in gray, white and light grey respectively. Black regions indicate the overlap of SP and US regions. To highlight the effect of FWM, we compare the stability regions with the cases for $F_i = 0$ and $s_1(t) = 0$. Their stability regions are calculated analytically starting from the characteristic equation of the eigenvalue problem and the US/SP borders are reported in orange and dashed red respectively.

When $F_i = 0$, FWM generation and, hence, the idler are neglected. The intensity-dependent effect of the signal is accounted for in the total intensity $I_T = I_0 + I_1$, affecting the thermal detuning and inducing cross-phase modulation (XPM) on the pump. When $s_1(t) = 0$, the system simply reduces to the well-known case of a single pump coupled to the cavity [7,27]. The unstable region can be observed for $\delta_0 < -\sqrt{3}$ or $\delta_0 > \sqrt{3}$ depending on the sign of ρ and for intra-cavity energies larger than $2\left|\sqrt{3}(\rho+1)\right|^{-1}$: below this value bi-stability cannot be observed for any detuning. SP can be found for:

$$\boldsymbol{\delta}_0^{SP} = \frac{2(1+\boldsymbol{\sigma})}{\boldsymbol{\rho} - 2\boldsymbol{\sigma}}\sqrt{\boldsymbol{\sigma}^{-1}(1+\boldsymbol{\rho})(\boldsymbol{\rho}(\boldsymbol{\sigma}-1)+3\boldsymbol{\sigma})}. \quad (3)$$

Eq. (4) implies that SP is rarely observed in micro-cavities having a thermo-optical coefficient of the same sign of the Kerr coefficient. In general, the SP region shrinks with σ, implying that SP is more difficult to observe on cavities with lower Q factor [7].

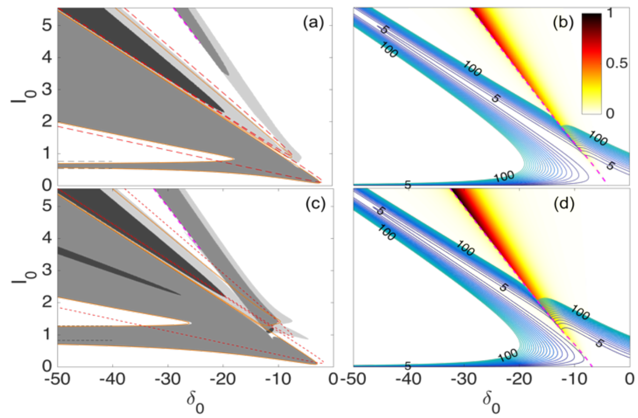

Fig. 1. Stability map (a,c) and stationary state (b,d) for $\sigma = 50, \rho = -10$. (a,b) $\delta_1 = -7; I_{+1} = 0.1$; (c,d) $\delta_1 = -12; I_{+1} = 0.2$. (a,c) Stable (S), unstable (US), self-pulsing (SP) and overlapping SP and US regions are in white, dark gray, light gray and black respectively. The boundaries of the S regions for $s_1(t) = 0$ and $F_i = 0$ are in dashed red and orange, respectively. Black and magenta dotted lines are Eq. (4,5), respectively. (b,d) Stationary state value for the lowest I_{-1} are reported in fake colors, nonlinear resonances are in blue for P_0 from 5 to 100.

A dramatic change of these stability regions occurs when a signal is coupled into the system. In the example of Fig. 1 we used a signal detuning $\delta_1 = -7, -12$ and an intra-cavity signal energy $I_{+1} = 0.1, 0.2$ for (a,b) and (c,d) respectively. It is important to stress that such energy values are small - comparable to the threshold $2\left|\sqrt{3}(\rho+1)\right|^{-1} \approx\ 0.12$ for observing any signal bi-stability when the pump is off. However, such an energy is enough to produce in the stability regions two relevant changes, when compared to the case of no-signal ($s_1(t) = 0$, red dashed lines).

First, the coupled signal creates a new tongue in the US region, purely related to the XPM and to the change in the detuning Δ induced by the signal. This is clearly visible when comparing the results with the regions where no FWM is present, $F_i = 0$ (orange). In the limit of large absolute pump detuning $|\delta_0| \gg 0$, the tongue is bounded by:

$$\boldsymbol{I}_0^{XPM\pm} = \frac{\boldsymbol{\delta}_1 - 2\mathbf{I}_1(1+\boldsymbol{\rho}) \pm \sqrt{\mathbf{I}_1^2(1+\boldsymbol{\rho})^2 - 1}}{2+\boldsymbol{\rho}}. \quad (4)$$

Eq. (4) approximates the analytical solution for $F_i = 0$. Unfortunately, these regions cannot be easily accessed experimentally at low intensities, requiring values $P_0 > 30$ in the examples reported. This is clear when looking at the iso-level curves of the stationary state for constant input pump powers (Fig. 1 (b,d), blue contour lines).

More relevantly, a new SP/US region appears where the FWM is stronger, i.e. where the stationary state has a large idler's intensity I_{-1} component (Fig. 1 (b,d), false color map). Roughly, such high generation occurs where the idler is resonantly coupled, i.e. $\delta_{-1} = (2+\rho)I_T - I_{-1}$, leading to:

$$\boldsymbol{\delta}_0 = \frac{\boldsymbol{\delta}_1}{2} + \frac{(2+\boldsymbol{\rho})\boldsymbol{I}_T - \boldsymbol{I}_{-1}}{2} \approx \frac{\boldsymbol{\delta}_1}{2} + \frac{\boldsymbol{I}_0(2+\boldsymbol{\rho})}{2}, \quad (5)$$

being the latter approximation valid for low $I_{\pm 1}$ intensities. Eq. (5) is plotted in Fig. 1 with a magenta dashed line for the specific cases. Notably, the latter SP/US region can be accessed for relatively low input pump powers, $P_0 > 3$. Finally, the eigenvalues and the stationary state reported in Fig. 1 are relative to the idler solution with the lowest energy. The idler mode can have up to three real solutions, which however are found only for high pump excitations, ($P_0 > 40$ in Fig. 1). In general, Eqs. (4,5) provide a useful mean to evaluate the regions that can be affected by the presence of the signal. In particular, Eq. (5) shows that the detuning δ_1 can be used to move the SP region in the I_0, δ_0 plane, as can be seen by comparing the stability maps in Fig. 1 (a,b) and (c,d) for $\delta_1 = -7$ and -12 respectively.

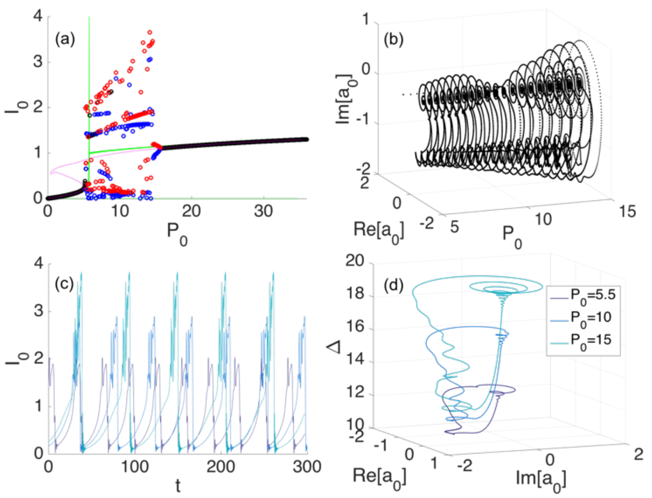

Fig. 2 Dynamical response for increasing values of P_0 for $\sigma = 50, \rho = -10, \delta_0 = -6.7, \delta_1 = -7, P_1 = 0.2$. (a) Bifurcation diagram of I_0 vs P_0, stable outputs are in black, the maxima and minima of the oscillatory output are in red and blue, respectively. Green is for $s_1 = 0$ and magenta is the stationary state. (b) Phase portrait of the bifurcation diagram, for P_0 against $\mathrm{Re}[a_0]$ and $\mathrm{Im}[a_0]$.Time evolution (c) of I_0 at $P_0 = 5.5$, 10, 15 for dark to light blue, respectively and long term phase plots (d) for Δ vs $\mathrm{Re}[a_0]$ and $\mathrm{Im}[a_0]$.

We studied the dynamics of Eqs. (1) using an adaptive 6th order Runge-Kutta solver [26]. We extended Eq.(2) to a secondary idler a_2, i.e. adding a term for $i = 2$, with $F_0 = 2\,a_0^* a_1 a_{-1} + a_1^2 a_2^* + 2a_1^* a_2 a_{-1}$, $F_1 = 2\,a_1^* a_2 a_0 + a_0^2 a_{-1}^* + 2a_0^* a_2 a_{-1}$, $F_{-1,2} = a_{0,1}^2 a_{1,0}^* + 2a_{2,-1}^* a_0 a_1$ and $I_T = \Sigma_{k=0,\pm1,2} I_k$. This allowed us to test the validity of our approach at higher pump and signal rates, which may arise in the self-pulsing regimes. Further cascaded generation is neglected here as the energies involved are low.

We carry out our analysis varying the input pump power P_0, for $\delta_0 = -6.7$. For such a detuning, in the case $s_1(t) = 0$ SP instability is never observed: from Eq. (3) we have that the maximum detuning for SP is $\delta_0^{SP} = -7.25$. We choose two different sets of parameters for the signal, $\delta_1 = -7, -12$ and $P_1 = 0.1, 0.9$ for Fig. 2 and 3, respectively. Here we plotted (a) the bifurcation diagrams associated to an hard excitation by varying the pump power P_0 from low to high values, (b,d) the phase portraits of the trajectories of interests and (c) the propagation in time of the intra-cavity fields. Although the two cases are obtained for the same pump parameters, they show a substantially different behavior.

In Fig. 2 the signal power and detuning have been chosen to observe a fold-Hopf bifurcation, which is obtained when the real parts of three leading eigenvalues, a real one and two complex conjugates (controlling the US and SP boundaries, respectively) change sign in proximity of the same value of the varying parameter, here P_0. Looking at the stationary state stability map in Fig. 1 (a), we see that the FWM-controlled SP and the US regions are in close proximity for $\delta_0 = -6.7$ and $I_0 \approx 1$: such a point belongs to the to the stationary curve with $P_0 \approx 5$ (Fig. 1 (b)), where we expect to find the fold-Hopf bifurcation.

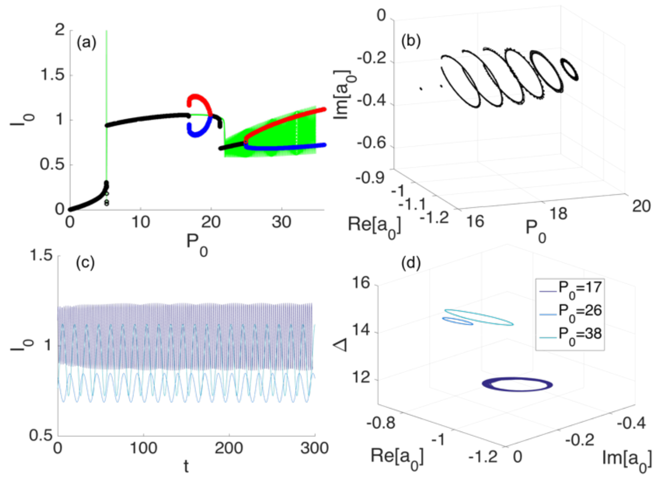

Fig. 3 Dynamical response for increasing values of P_0 for $\sigma = 50, \rho = -10, \delta_0 = -6.7, \delta_1 = -12, P_1 = 0.9$. (a) Bifurcation diagram of I_0 vs P_0, stable outputs are in black, the maxima and minima of the oscillatory output are in red and blue, respectively. The green plot corresponds to $F_i = 0$. (b)) Phase portrait of the bifurcation diagram, for P_0 against $\mathrm{Re}[a_0]$ and $\mathrm{Im}[a_0]$. Time evolution (c) of I_0 at $P_0 = 17, 25, 38$ (dark to light blue, respectively) and long term phase plots (d) for Δ vs $\mathrm{Re}[a_0]$ and $\mathrm{Im}[a_0]$.

Fig. 2(a) reports I_0 vs P_0 for the stationary state (magenta), for the dynamical response of the full system (in black for the stable case and in red and blue for the maxima and minima of the oscillating cases) and of the system with $s_1(t) = 0$ (green curve). Starting from low power, the system moves along the stationary state until it approaches the switching threshold at $P_0 > 5$. Here, for $s_1(t) = 0$ the system switches but, as expected, does not oscillate. Conversely, the full system exhibits the expected heteroclinic bifurcation from a saddle point to saddle-focus trajectory (fold-Hopf) at $P_0 = 5$ and, eventually, a homoclinic bifurcation to a focus at $P_0 = 15$ (Fig. 2 (b)). The fold-Hopf bifurcation converges to a stable limit. Such a phase orbit is a homoclinic saddle-focus (Shilnikov) trajectory, which jumps between low and high values of the slow detuning Δ (Fig. 2 (d)). For a thermal nonlinearity, this means that the temperature of the system oscillates, mostly between two points. Such a trajectory results in the formation of large pulses (Fig. 2(c)), typical of this type of bifurcation, featuring ripples due to the presence of the focus in the trajectory. Giant pulse generation has recently been studied in thermal systems with two relaxation constants [11].

A completely different scenario is obtained in the case of Fig. 3, where the FWM controlled SP region is far from the US region (see Fig. 1 (b) for $\delta_0 = -6.7$). In this case, the system experiences first

($P_0 = 5$) a saddle-node bifurcation, characteristic of bistable systems and ruled by a single leading real eigenvalue that changes sign, similarly to the case $s_1(t) = 0$. At higher powers ($P_0 = 15$) it goes to a homoclinic Hopf (Andronov-Hopf) bifurcation. Here a couple of complex conjugate leading eigenvalues changes sign, resulting in a smooth cycle (Fig. 3 (b)). The real and imaginary parts ($\mathrm{Re}[a_0], \mathrm{Im}[a_0]$) of the pump amplitude (Fig. 3 (d) dark blue) do not present significant oscillation in the detuning region, resulting in a clean periodical oscillation (Fig. 3 (c) dark blue). The system bifurcates again to a stable focus at $P_0 = 18$, while a new Hopf bifurcation appears for $P_0 > 25$ where the real part of another set of complex conjugate eigenvalues changes sign. In this case the phase portraits (Fig. 3 (d), light blue) show an oscillation also in the detuning plane. This last bifurcation belongs to an SP region that appears also when the effect of the FWM is disregarded (green curve in Fig. 3 (a)). FWM, however, contributes to modify its domain of existence.

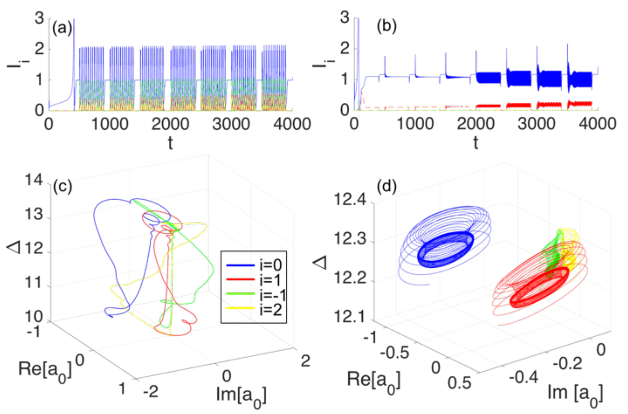

Fig. 4. Time evolution for repeatedly on/off P_1 signal for $\sigma = 50, \rho = -10, \delta_0 = -6.7$. The range of parameters is chosen in the SP regions of Fig. 2 for (a,c), $P_0 = 6, \delta_1 = -7$ and of Fig. 3 for (b,d) $P_0 = 18, \delta_1 = -12$. Blue, red, green and yellow are for the pump and signal first and second idler, respectively. (a,b) report the time response for the intra-cavity energies. P_1 is turned on and off repeatedly, with power linearly increasing from 0.1 to 0.4 and from 0.1 to 0.6 in (a) and (b) respectively. (c,d) reports a typical long term phase portrait for $P_1 = 0.3$ and 0.5, respectively, showing the homoclinic saddle-focus (Shilnikov) and circular trajectories.

The presence of the signal allows to observe higher order bifurcations where the system was previously stable. This is the case of the fold-Hopf bifurcation of Fig. 2, which is obtained only when more than one leading eigenvalue is available in the bifurcation region. It is interesting to observe how the system responds to on-off signal inputs, as shown in Fig. 4 for different signal input powers. Selecting the parameters within the SP regions discussed in Fig. 2-3, a homoclinic saddle-focus (Shilnikov) and circular trajectories can be achieved for a range of parameters.

In conclusion, we propose a novel approach, based on parametric FMW interaction, for controlling self- pulsation and bifurcation in micro-cavities featuring a time-dependent nonlinearity. These results are general and show that the degenerate FWM can induce a new set of bifurcations that can be relocated in the space of parameters by acting on the power and frequency of the control signal. We show that the possibility of moving the stability regions and, especially, to place at will the crossing boundaries has profound implications on the dynamical response of the system. Our study paves the way for enhanced, low-power all-optical control for sensors, oscillators and chaos controlled devices, adding new and flexible degrees of freedom to the system. Such an approach is also relevant for gaining new understanding in micro-comb applications, where the control of the thermal response is critical.

Acknowledgment. We acknowledge the support of the U.K. Quantum Technology Hub for Sensors and Metrology, EPSRC, under Grant EP/M013294/1, of the Marie Curie Action MC-CIG and IIF REA grant 630833 and 327627. RM acknowledges support from the CRC, NSERC and MEIE, the ITMO and Professorship Program (grant 074-U 01) and the 1000 Talents Sichuan Program.

References

1. K. J. Vahala, Nature **424**, 839–846 (2003).
2. A. B. Matsko, and V. S. Ilchenko, IEEE J. of Select.Topics Quantum Electron., **12**, 3-14 (2006).
3. V. S. Ilchenko, and M. L. Gorodetskii, Laser Phys. **2**, 1004–1009 (1992).
4. T. Carmon, L. Yang, and K. J. Vahala, Opt. Express **12**, 4742–4750 (2004).
5. F. Monifi, J. Zhang, S.K. Özdemir, B. Peng, Y.-X.Liu, F. Bo, F. Nori, and L. Yang, Nat. Photon. **10**, 399-405 (2016).
6. S. Malaguti, G. Bellanca, A. De Rossi, S. Combrié, and S. Trillo, Phys Rev. A , **83** 051802 (2011).
7. A. E. Fomin, M. L. Gorodetski, I. S. Grudinin, and V. S. Ilchenko, J. Opt. Soc. Am. B **22**, 469 (2006).
8. I. S. Grudinin, and K. J. Vahala, Opt. Express **17**, 14088 (2009).
9. L. He, Y.-F. Xiao, J. Zhu, S. K. Ozdemir, and L. Yang, Opt. Express **17**, 9571–9581 (2009).
10. Y. S. Park, and H. Wang, Opt. Lett. **32**, 3104–3106 (2007).
11. S. Diallo, G. Lin, and Y. K. Chembo, Opt. Lett. **40**, 3834-3837 (2015).
12. Y. Deng, F. Liu, Z. C. Leseman, and M. Hossein-Zadeh, Opt. Express **21**, 4653-4664 (2013).
13. T. Kippenberg, R. Holzwarth, and S. Diddams, Science **332**, 555 (2011) and reference therin.
14. T. Herr, V. Brasch, J. D. Jost, C. Y. Wang, N. M. Kondratiev, M. L. Gorodetsky, and T. J. Kippenberg, Nat. Photonics **8**, 145–152 (2014).
15. C. Joshi, et al., Opt. Lett. **41,** 2565–2568 (2016).
16. V. E. Lobanov, G. V. Lihachev, N. G. Pavlov, A. V. Cherenkov, T. J. Kippenberg, and M. L. Gorodetsky, Opt. Express **24**, 27382-27394 (2016).
17. Ö. Boyraz, P. Koonath, V. Raghunathan, and B. Jalali, Opt. Express **12**, 4094-4102 (2004).
18. P. Kumar et al. J. Phys. B: At. Mol. Opt. Phys. **42** 145401, (2009).
19. T. J. Johnson, M. Borselli, and O. Painter,Opt. Express **14**, 817–831 (2006).
20. W. H. Pernice, M. Li, and H. X. Tang, Opt. Express **18**, 18438–18452 (2010).
21. C. Baker et al. Opt. Express **20,** 29076–29089 (2012).
22. L. H. Nguyen, and K.-S. Hong, Phys. Lett. A **376,** 442-446, (2012) and reference therin.
23. D. Ceoldo, A. Bendahmane, J. Fatome, G. Millot, T. Hansson, D. Modotto, S. Wabnitz, and B. Kibler, Opt. Lett. **41**, 5462-5465 (2016).
24. A. Pasquazi et al., Opt. Express **21**, 13333-13341 (2013).
25. H. A. Haus, Waves and Fields in Optoelectronics (Prentice-Hall, 1983).
26. Y. A. Kuznetsov, “Elements of applied bifurcation theory,” Springer-Verlag New York, (1998).
27. The boundaries for the U and SP regions are respectively [7] : $I_0^{U,\pm} = \left(2\delta_0 \pm \sqrt{\delta_0^2 - 3}\right) 3^{-1}(1+\rho)^{-1}$, and $I_0^{SP,\pm} = \frac{\delta_0(2(2+\rho)\sigma-\rho)}{2(1+\rho)(\rho(\sigma-1)+3\sigma)} \pm \sqrt{\frac{\delta_0^2(2(2+\rho)\sigma-\rho)^2}{4(1+\rho)^2(\rho(\sigma-1)+3\sigma)^2} - \frac{1+\sigma(2+\sigma+\delta_0^2\sigma)}{\sigma(1+\rho)(\rho(\sigma-1)+3\sigma)}}$.

References

Set references at the back of the manuscript. *Optics Letters* uses an abbreviated reference style. Citations to journal articles should omit the article title and final page number. However, full references (to aid the editor and reviewers) must be included as well on a fifth page that will not count against page length.

1. K. J. Vahala, “Optical microcavities,” Nature **424**, 839–846 (2003).
2. A. B. Matsko and V. S. Ilchenko, "Optical resonators with whispering-gallery modes-part I: basics," IEEE J. of Select.Topics Quantum Electron , **12**, 3-14 (2006).
3. V. S. Ilchenko and M. L. Gorodetskii, “Thermal nonlinear effects in optical whispering gallery microresonators,” Laser Phys. 2, 1004–1009 (1992).
4. T. Carmon, L. Yang, and K. J. Vahala, “Dynamical thermal behavior and thermal self-stability of microcavities,” Opt. Express **12**(20), 4742–4750 (2004).
5. F. Monifi, J. Zhang, S.K. Özdemir, B. Peng, Y.-X.Liu, F. Bo, F. Nori, L. Yang, L., “Optomechanically induced stochastic resonance and chaos transfer between optical fields”, Nat. Photon. **10**, 399-405 (2016).
6. S. Malaguti, G. Bellanca, A. De Rossi, S. Combrié, S. Trillo, “Self-pulsing driven by two-photon absorption in semiconductor nanocavities”, Phys Rev. A , **83** 051802 (2011).
7. A. E. Fomin, M. L. Gorodetski, I. S. Grudinin, and V. S. IIchenko, J. Opt. Soc. Am. B 22, 469 (2006).
8. I. S. Grudinin and K. J. Vahala, Opt. Express **17**, 14088 (2009).
9. L. He, Y.-F. Xiao, J. Zhu, S. K. Ozdemir, and L. Yang, “Oscillatory thermal dynamics in high-Q PDMS-coated silica toroidal microresonators,” Opt. Express **17**(12), 9571–9581 (2009).
10. Y. S. Park and H. Wang, “Regenerative pulsation in silica microspheres,” Opt. Lett. 32(21), 3104–3106 (2007)
11. S. Diallo, G. Lin, and Y. K. Chembo, "Giant thermo-optical relaxation oscillations in millimeter-size whispering gallery mode disk resonators," Opt. Lett. **40**, 3834-3837 (2015)
12. Yang Deng, Fenfei Liu, Zayd C. Leseman, and Mani Hossein-Zadeh, "Thermo-optomechanical oscillator for sensing applications," Opt. Express 21, 4653-4664 (2013).
13. T. Kippenberg, R. Holzwarth, and S. Diddams, Science 332, 555 (2011) and reference therin.
14. T. Herr, V. Brasch, J. D. Jost, C. Y. Wang, N. M. Kondratiev, M. L. Gorodetsky, T. J. Kippenberg, “Temporal solitons in optical microresonators”, Nat. Photonics 8 (2014) 145–152.
15. C. Joshi, J. K. Jang, K. Luke, X. Ji, S. A. Miller, A. Klenner, Y. Okawachi, M. Lipson, A. L. Gaeta, “Thermally controlled comb generation and soliton modelocking in microresonators”, Opt. Lett. **41** 2565–2568 (2016)
16. V. E. Lobanov, G. V. Lihachev, N. G. Pavlov, A. V. Cherenkov, T. J. Kippenberg, and M. L. Gorodetsky, "Harmonization of chaos into a soliton in Kerr frequency combs," Opt. Express **24**, 27382-27394 (2016)
17.Ö. Boyraz, P. Koonath, V. Raghunathan, and B. Jalali, "All optical switching and continuum generation in silicon waveguides," Opt. Express **12**, 4094-4102 (2004).
18. P. Kumar, A. Prasad, and R. Ghosh, “Strange bifurcation and phase-locked dynamics in mutually coupled diode laser systems,” J. Phys. B: At. Mol. Opt. Phys. **42** 145401, (2009)
19. T. J. Johnson, M. Borselli, and O. Painter, “Self-induced optical modulation of the transmission through a highQ silicon microdisk resonator,” Opt. Express **14**(2), 817–831 (2006).
20. W. H. Pernice, M. Li, and H. X. Tang, “Time-domain measurement of optical transport in silicon micro-ring resonators,” Opt. Express **18**, 18438–18452 (2010).
21. C. Baker, S. Stapfner, D. Parrain, S. Ducci, G. Leo, E. M. Weig, and I. Favero, “Optical instability and selfpulsing in silicon nitride whispering gallery resonators,” Opt. Express **20,** 29076–29089 (2012).
22. L. H. Nguyen, K.-S. Hong, “Hopf bifurcation control via a dynamic state-feedback control”, Phys. Lett. A **376** 442-446, (2012) and reference therin
23. D. Ceoldo, A. Bendahmane, J. Fatome, G. Millot, T. Hansson, D. Modotto, S. Wabnitz, and B. Kibler, "Multiple four-wave mixing and Kerr combs in a bichromatically pumped nonlinear fiber ring cavity," Opt. Lett. **41**, 5462-5465 (2016).
24. A. Pasquazi, L. Caspani, M. Peccianti, M. Clerici, M. Ferrera, L. Razzari, D. Duchesne, B. E. Little, S. T. Chu, D. J. Moss, and R. Morandotti, "Self-locked optical parametric oscillation in a CMOS compatible microring resonator: a route to robust optical frequency comb generation on a chip," Opt. Express **21**, 13333-13341 (2013).
25. H. A. Haus, Waves and Fields in Optoelectronics (Prentice-Hall, 1983).
26. Y. A. Kuznetsov, “Elements of applied bifurcation theory,” Springer-Verlag New York, (1998)
27. Following Ref. [7], the boundaries for the unstable and SP regions are : $I_0^{U,\pm} = \left(2\delta_0 \pm \sqrt{\delta_0^2 - 3}\right) 3^{-1}(1+\rho)^{-1}$, and $I_0^{SP,\pm} = \frac{\delta_0(2(2+\rho)\sigma-\rho)}{2(1+\rho)(\rho(\sigma-1)+3\sigma)} \pm \sqrt{\frac{\delta_0^2(2(2+\rho)\sigma-\rho)^2}{4(1+\rho)^2(\rho(\sigma-1)+3\sigma)^2} - \frac{1+\sigma(2+\sigma+\delta_0^2\sigma)}{\sigma(1+\rho)(\rho(\sigma-1)+3\sigma)}}$ respectively.